Measurement of the moments of the photon energy spectrum in $B \to X_s\gamma$ decays and determination of $|V_{cb}|$ and m_b at Belle

C. Schwanda,[10] P. Urquijo,[20] E. Barberio,[20] A. Limosani,[20] I. Adachi,[7] H. Aihara,[42] K. Arinstein,[1] T. Aushev,[17,12] S. Bahinipati,[2] A. M. Bakich,[38] V. Balagura,[12] I. Bedny,[1] K. Belous,[11] U. Bitenc,[13] A. Bondar,[1] A. Bozek,[26] M. Bračko,[19,13] M.-C. Chang,[3] A. Chen,[23] W. T. Chen,[23] B. G. Cheon,[5] R. Chistov,[12] I.-S. Cho,[47] Y. Choi,[37] J. Dalseno,[20] M. Dash,[46] A. Drutskoy,[2] S. Eidelman,[1] B. Golob,[18,13] H. Ha,[15] J. Haba,[7] T. Hara,[31] K. Hayasaka,[21] H. Hayashii,[22] M. Hazumi,[7] D. Heffernan,[31] Y. Hoshi,[40] W.-S. Hou,[25] H. J. Hyun,[16] K. Inami,[21] A. Ishikawa,[34] H. Ishino,[43] R. Itoh,[7] M. Iwasaki,[42] Y. Iwasaki,[7] D. H. Kah,[16] J. H. Kang,[47] P. Kapusta,[26] N. Katayama,[7] H. Kichimi,[7] H. J. Kim,[16] Y. J. Kim,[4] K. Kinoshita,[2] S. Korpar,[19,13] Y. Kozakai,[21] P. Križan,[18,13] P. Krokovny,[7] R. Kumar,[32] C. C. Kuo,[23] Y. Kuroki,[31] A. Kuzmin,[1] Y.-J. Kwon,[47] J. S. Lee,[37] M. J. Lee,[36] S. E. Lee,[36] T. Lesiak,[26] J. Li,[6] C. Liu,[35] D. Liventsev,[12] F. Mandl,[10] A. Matyja,[26] S. McOnie,[38] T. Medvedeva,[12] W. Mitaroff,[10] H. Miyake,[31] H. Miyata,[28] Y. Miyazaki,[21] R. Mizuk,[12] G. R. Moloney,[20] E. Nakano,[30] M. Nakao,[7] Z. Natkaniec,[26] S. Nishida,[7] O. Nitoh,[45] S. Noguchi,[22] T. Nozaki,[7] S. Ogawa,[39] T. Ohshima,[21] S. Okuno,[14] P. Pakhlov,[12] G. Pakhlova,[12] H. Palka,[26] C. W. Park,[37] H. Park,[16] L. S. Peak,[38] R. Pestotnik,[13] L. E. Piilonen,[46] H. Sahoo,[6] Y. Sakai,[7] O. Schneider,[17] J. Schümann,[7] R. Seidl,[8,33] A. Sekiya,[22] K. Senyo,[21] M. E. Sevior,[20] M. Shapkin,[11] H. Shibuya,[39] J.-G. Shiu,[25] B. Shwartz,[1] A. Somov,[2] S. Stanič,[29] M. Starič,[13] T. Sumiyoshi,[44] F. Takasaki,[7] M. Tanaka,[7] G. N. Taylor,[20] Y. Teramoto,[30] I. Tikhomirov,[12] K. Trabelsi,[7] S. Uehara,[7] Y. Unno,[5] S. Uno,[7] G. Varner,[6] K. E. Varvell,[38] K. Vervink,[17] S. Villa,[17] C. H. Wang,[24] P. Wang,[9] Y. Watanabe,[14] R. Wedd,[20] E. Won,[15] B. D. Yabsley,[38] H. Yamamoto,[41] Y. Yamashita,[27] Z. P. Zhang,[35] and A. Zupanc[13]

(Belle Collaboration)

[1]*Budker Institute of Nuclear Physics, Novosibirsk*
[2]*University of Cincinnati, Cincinnati, Ohio 45221, USA*
[3]*Department of Physics, Fu Jen Catholic University, Taipei*
[4]*The Graduate University for Advanced Studies, Hayama*
[5]*Hanyang University, Seoul*
[6]*University of Hawaii, Honolulu, Hawaii 96822, USA*
[7]*High Energy Accelerator Research Organization (KEK), Tsukuba*
[8]*University of Illinois at Urbana-Champaign, Urbana, Illinois 61801, USA*
[9]*Institute of High Energy Physics, Chinese Academy of Sciences, Beijing*
[10]*Institute of High Energy Physics, Vienna*
[11]*Institute of High Energy Physics, Protvino*
[12]*Institute for Theoretical and Experimental Physics, Moscow*
[13]*J. Stefan Institute, Ljubljana*
[14]*Kanagawa University, Yokohama*
[15]*Korea University, Seoul*
[16]*Kyungpook National University, Taegu*
[17]*École Polytechnique Fédérale de Lausanne (EPFL), Lausanne*
[18]*Faculty of Mathematics and Physics, University of Ljubljana, Ljubljana*
[19]*University of Maribor, Maribor*
[20]*University of Melbourne, School of Physics, Victoria 3010*
[21]*Nagoya University, Nagoya*
[22]*Nara Women's University, Nara*
[23]*National Central University, Chung-li*
[24]*National United University, Miao Li*
[25]*Department of Physics, National Taiwan University, Taipei*
[26]*H. Niewodniczanski Institute of Nuclear Physics, Krakow*
[27]*Nippon Dental University, Niigata*
[28]*Niigata University, Niigata*
[29]*University of Nova Gorica, Nova Gorica*
[30]*Osaka City University, Osaka*
[31]*Osaka University, Osaka*
[32]*Panjab University, Chandigarh*
[33]*RIKEN BNL Research Center, Upton, New York 11973, USA*
[34]*Saga University, Saga*
[35]*University of Science and Technology of China, Hefei*

[36]*Seoul National University, Seoul*
[37]*Sungkyunkwan University, Suwon*
[38]*University of Sydney, Sydney, New South Wales*
[39]*Toho University, Funabashi*
[40]*Tohoku Gakuin University, Tagajo*
[41]*Tohoku University, Sendai*
[42]*Department of Physics, University of Tokyo, Tokyo*
[43]*Tokyo Institute of Technology, Tokyo*
[44]*Tokyo Metropolitan University, Tokyo*
[45]*Tokyo University of Agriculture and Technology, Tokyo*
[46]*Virginia Polytechnic Institute and State University, Blacksburg, Virginia 24061, USA*
[47]*Yonsei University, Seoul*
(Received 10 March 2008; published 27 August 2008)

Using the previous Belle measurement of the inclusive photon energy in $B \to X_s\gamma$ decays, we determine the first and second moments of this spectrum for minimum photon energies in the B meson rest frame ranging from 1.8 to 2.3 GeV. Combining these measurements with recent Belle data on the lepton energy and hadronic mass moments in $B \to X_c\ell\nu$ decays, we perform fits to theoretical expressions derived in the 1S and kinetic mass schemes and extract the magnitude of the Cabibbo-Kobayashi-Maskawa matrix element V_{cb}, the b-quark mass, and other nonperturbative parameters. In the 1S scheme analysis we find $|V_{cb}| = (41.56 \pm 0.68(\text{fit}) \pm 0.08(\tau_B)) \times 10^{-3}$ and $m_b^{1S} = (4.723 \pm 0.055)$ GeV. In the kinetic scheme, we obtain $|V_{cb}| = (41.58 \pm 0.69(\text{fit}) \pm 0.08(\tau_B) \pm 0.58(\text{th})) \times 10^{-3}$ and $m_b^{\text{kin}} = (4.543 \pm 0.075)$ GeV.

DOI: 10.1103/PhysRevD.78.032016 PACS numbers: 12.15.Ff, 12.15.Hh, 12.39.Hg, 13.20.He

I. INTRODUCTION

The most precise determinations of the Cabibbo-Kobayashi-Maskawa (CKM) matrix element $|V_{cb}|$ [1] are obtained using combined fits to inclusive B decay distributions [2–5]. These analyses are based on calculations of the semileptonic decay rate and spectral moments in $B \to X_c\ell\nu$ and $B \to X_s\gamma$ decays in the frameworks of the operator product expansion (OPE) and the heavy quark effective theory (HQET) [2,6–8], which predict these quantities in terms of $|V_{cb}|$ and a number of nonperturbative heavy quark (HQ) parameters including the b-quark mass m_b.

Analyses combining measurements from different experiments [2,3] quote the most precise numbers for $|V_{cb}|$ and m_b. However, as the correlated systematic uncertainties are not precisely known, there is some concern that uncertainties are underestimated. In this analysis, we have chosen the opposite approach and perform fits to the data from the Belle experiment only. In addition, we use two independent sets of theoretical expressions, derived in the 1S [2] and kinetic mass [7,8] schemes respectively, to test the compatibility of these two frameworks.

The present document is organized as follows: Sec. II describes the measurement of the first and second moment of the inclusive photon energy spectrum in $B \to X_s\gamma$, $\langle E_\gamma \rangle$, and $\langle (E_\gamma - \langle E_\gamma \rangle)^2 \rangle$, using the Belle measurement of this decay in Ref. [9]. In the previously published analysis the first and second moments were obtained for one value of the minimum energy threshold, namely $E_{\text{min}} = 1.8$ GeV. Here we report additional measurements with $E_{\text{min}} = 1.9$, 2.0, 2.1, 2.2, 2.3 GeV, and perform a reevaluation of the systematic error. In Sec. III we use these data together with the recent Belle measurements of the lepton energy and hadronic mass moments in $B \to X_c\ell\nu$ decays [10,11] to extract $|V_{cb}|$ and m_b using theoretical expressions derived in the 1S and kinetic mass schemes.

II. MOMENTS OF THE $B \to X_s\gamma$ PHOTON ENERGY SPECTRUM

A. Review of the Belle $B \to X_s\gamma$ measurement

The analysis described in Ref. [9] uses $e^+e^- \to \Upsilon(4S) \to B\bar{B}$ events equivalent to 140 fb^{-1} of integrated luminosity (ON sample) and 15 fb^{-1} taken 60 MeV below the $\Upsilon(4S)$ resonance energy (OFF sample). Photon candidates with energy greater than 1.5 GeV as measured in the $\Upsilon(4S)$ rest frame are reconstructed. Vetoes are applied to photon candidates with high likelihood of originating from π^0 or η decays to two photons.

In general, the background of photons from the $e^+e^- \to q\bar{q}$ continuum is dominant. It is suppressed with event shape variables used as the inputs to two Fisher discriminants [12]. The first discriminant distinguishes spherically shaped $B\bar{B}$ from jetlike continuum events and includes the Fox-Wolfram moments [13], the thrust calculated using all particles detected in the event including and excluding the candidate photon, and the angles of the corresponding

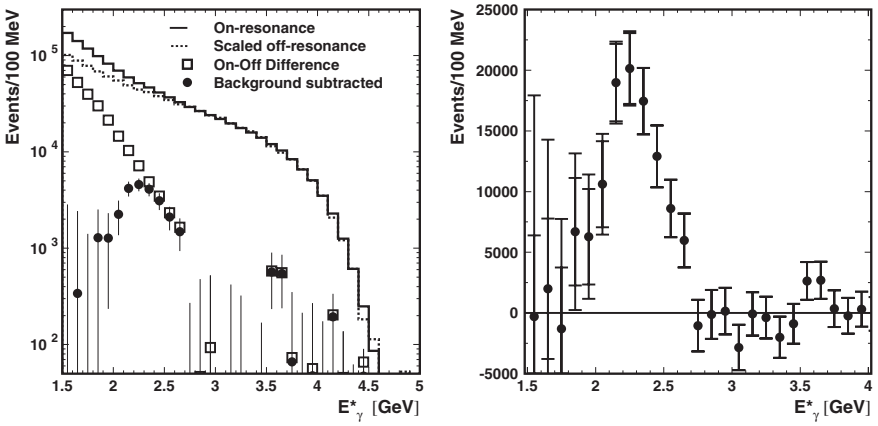

FIG. 1. Left: raw photon energy spectrum in the $\Upsilon(4S)$ frame; right: photon energy spectrum after background subtraction and efficiency correction where the inner error bars are the statistical uncertainties and the outer error bars show the total errors, which include the systematic uncertainties. These plots are reproduced from Ref. [9].

thrust axes with respect to the beam and candidate photon directions, respectively. The second discriminant is designed to exploit the topology of $B \to X_s\gamma$ events by utilizing the energy sum of detected particles, which is measured in three angular regions bounded by cones that are subtended from the direction of the candidate photon in the $\Upsilon(4S)$ frame; defined as 0°–30° (forward), 30°–140° (middle), and 140°–180° (backward).

After these selections are applied, the remaining continuum background is removed by subtracting scaled OFF data from the ON data set. Backgrounds in $B\bar{B}$ events, including photons from π^0 and η (veto leakage), other real photons (mainly from ω, η', and J/ψ), clusters in the calorimeter not due to single photons (mainly electrons interacting with matter, K_L^0 and $\bar{n}$), and beam background, are estimated from Monte Carlo (MC) simulation (Fig. 1).

B. Moment measurements

We calculate the truncated first and second moments, $\langle E_\gamma\rangle$ and $\langle(E_\gamma - \langle E_\gamma\rangle)^2\rangle$, of the efficiency corrected spectrum in Fig. 1 for minimum photon energies ranging from 1.8 to 2.3 GeV. The following corrections are applied to these moments: The nonzero B meson momentum in the $\Upsilon(4S)$ rest frame changes the first moment of the photon energy by 0.2% and adds a Doppler broadening of 0.006 GeV^2 to the second moment; the finite energy resolution, uncorrected in Fig. 1, causes a broadening of the spectrum and increases the second moment by 0.004 GeV^2; the 100 MeV binning in Fig. 1 increases the second moment by 0.0008 GeV^2.

The above corrections assume a symmetric photon energy distribution, and do not account for expected and known asymmetries in the true spectrum and detector response, respectively. To account for these effects an additional bias correction, derived from a MC simulation, is implemented. The $B \to X_s\gamma$ model contains decays of the form $B \to K^*\gamma$, where K^* is any known spin-1 resonance with strangeness $S = 1$. The relative amounts of these decays are adjusted by matching the total photon spectrum to the theoretical model of Ref. [14]. The bias correction, calculated as the difference of the true moment and the moment measured in the $B \to X_s\gamma$ MC simulation once all aforementioned corrections are applied, is listed in Table I.

C. Systematic uncertainties

The error bars of the efficiency corrected spectrum of Fig. 1 show the total error including the systematic uncertainty related to the scaling of the MC background samples (sizable in the first energy bins). In the calculation of the moments, we consider also the following sources of systematic uncertainty: uncertainty in the OFF data scaling factor; possible difference in ON and OFF data selection efficiencies; uncertainty in the $B\bar{B}$ data/MC correction; we vary by ±20% the background from η', ω and bremsstrahlung; uncertainty of the η veto efficiency; we consider an alternate signal MC that favors high-mass resonances decaying into high-multiplicity final states, where the fraction of $\gamma K\pi$ final states, somewhat overestimated in our default sample, matches our previous measurement [15]; and we vary the photon detection efficiency in both signal

TABLE I. Residual bias correction to $\langle E_\gamma\rangle$ and $\langle(E_\gamma - \langle E_\gamma\rangle)^2\rangle$ as a function of $E_{\rm min}$.

$E_{\rm min}$ (GeV)	$\Delta\langle E_\gamma\rangle$	$\Delta\langle(E_\gamma - \langle E_\gamma\rangle)^2\rangle$
1.8	+2.0%	0.0%
1.9	+1.6%	−0.4%
2.0	+1.2%	−7.1%
2.1	+0.8%	−17.4%
2.2	+0.2%	−35.3%
2.3	−0.3%	−57.9%

TABLE II. Systematic uncertainties contributing to the first moment $\langle E_\gamma \rangle$ as a function of the lower energy threshold $E_{\rm min}$ in GeV.

$E_{\rm min}$ (GeV)	1.8	1.9	2.0	2.1	2.2	2.3
MC scaling	0.021	0.012	0.006	0.003	0.002	0.001
OFF scaling	0.004	0.001	0.001	0.002	0.002	0.002
ON/OFF efficiency	0.000	0.000	0.000	0.000	0.000	0.000
$B\bar{B}$ data/MC correction	0.005	0.003	0.002	0.001	0.000	0.000
Other γs in $B\bar{B}$	0.010	0.004	0.002	0.000	0.000	0.000
η veto efficiency	0.001	0.001	0.000	0.000	0.000	0.000
Signal MC	0.004	0.004	0.004	0.004	0.004	0.003
γ efficiency	0.001	0.001	0.000	0.000	0.000	0.000
Bias correction	0.022	0.018	0.014	0.009	0.002	0.003
Total systematic	0.033	0.023	0.016	0.010	0.005	0.004

TABLE III. Systematic uncertainties contributing to the second moment $\langle (E_\gamma - \langle E_\gamma \rangle)^2 \rangle$ as a function of the lower energy threshold $E_{\rm min}$ in GeV^2.

$E_{\rm min}$ (GeV)	1.8	1.9	2.0	2.1	2.2	2.3
MC scaling	0.0060	0.0027	0.0009	0.0003	0.0001	0.0001
OFF scaling	0.0018	0.0010	0.0006	0.0005	0.0005	0.0004
ON/OFF efficiency	0.0000	0.0000	0.0000	0.0000	0.0000	0.0000
$B\bar{B}$ data/MC correction	0.0010	0.0004	0.0001	0.0000	0.0000	0.0000
Other γs in $B\bar{B}$	0.0024	0.0008	0.0002	0.0000	0.0000	0.0000
η veto efficiency	0.0003	0.0001	0.0000	0.0000	0.0000	0.0000
Signal MC	0.0007	0.0005	0.0004	0.0003	0.0002	0.0000
γ efficiency	0.0003	0.0001	0.0000	0.0000	0.0000	0.0000
Energy resolution	0.0020	0.0020	0.0021	0.0022	0.0023	0.0024
Binning	0.0008	0.0008	0.0008	0.0008	0.0008	0.0008
Bias correction	0.0068	0.0040	0.0026	0.0005	0.0004	0.0011
Total systematic	0.0099	0.0055	0.0036	0.0024	0.0025	0.0028

and background samples by its measured uncertainty ($\pm$ 2.3%).

We also assign systematic uncertainties to the corrections applied to the moments: an alternate energy resolution correction that neglects the lower energy tail in the resolution is implemented and the difference is assigned as systematic uncertainty; a $\pm$100% uncertainty on the binning correction for the second moment is assigned; we also implement a $\pm$50% variation on the bias correction for the first moment while for the second moment the correction is recalculated using the alternate signal MC sample.

The total systematic uncertainty on each moment measurement is obtained by summing the aforementioned contributions in quadrature (Tables II and III).

D. Results

The measurements of the first and second moments of the photon energy spectrum in $B \to X_s \gamma$ for minimum

TABLE IV. Measurements of $\langle E_\gamma \rangle$ and $\langle (E_\gamma - \langle E_\gamma \rangle)^2 \rangle$ as a function of the minimum photon energy $E_{\rm min}$. The first error is statistical and the second is systematic.

$E_{\rm min}$ (GeV)	$\langle E_\gamma \rangle$ (GeV)	$\langle (E_\gamma - \langle E_\gamma \rangle)^2 \rangle$
1.8	2.292 $\pm$ 0.027 $\pm$ 0.033	0.0305 $\pm$ 0.0079 $\pm$ 0.0099
1.9	2.309 $\pm$ 0.023 $\pm$ 0.023	0.0217 $\pm$ 0.0060 $\pm$ 0.0055
2.0	2.324 $\pm$ 0.019 $\pm$ 0.016	0.0179 $\pm$ 0.0050 $\pm$ 0.0036
2.1	2.346 $\pm$ 0.017 $\pm$ 0.010	0.0140 $\pm$ 0.0046 $\pm$ 0.0024
2.2	2.386 $\pm$ 0.018 $\pm$ 0.005	0.0091 $\pm$ 0.0045 $\pm$ 0.0025
2.3	2.439 $\pm$ 0.020 $\pm$ 0.004	0.0036 $\pm$ 0.0045 $\pm$ 0.0028

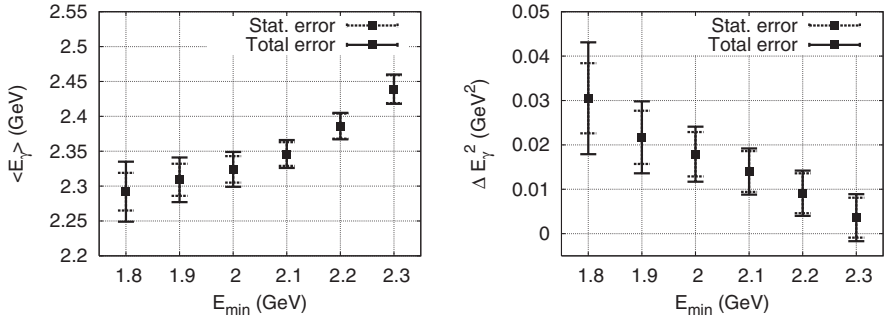

FIG. 2. Measurements of $\langle E_\gamma \rangle$ and $\langle (E_\gamma - \langle E_\gamma \rangle)^2 \rangle$ as a function of the minimum photon energy $E_{\rm min}$ ($\Delta E_\gamma^2 = \langle (E_\gamma - \langle E_\gamma \rangle)^2 \rangle$).

photon energies ranging from 1.8 GeV to 2.3 GeV are shown in Table IV and Fig. 2. Our results agree with the data from CLEO [16] and *BABAR* [17].

The statistical and systematic errors on the first and second moments at $E_{\rm min} = 1.8$ GeV are slightly different from the values quoted in Ref. [9] and supersede our previously published values. The change in the uncertainties is due to the use of the toy MC approach and to the additional contribution from the uncertainty in the bias correction.

The correlations between the different moment measurements are estimated using a toy MC approach: Starting from the efficiency corrected spectrum in Fig. 1 we create new spectra by generating values of a Gaussian random variable for the contents of each bin, where the mean and standard deviation of the Gaussian correspond to the bin yield and its uncertainty in the original spectrum. The moments and their fluctuations with respect to each other were measured for each generated spectrum, and finally averaged to yield the covariance matrix, from which the uncertainties due to statistics and systematics scaling were obtained. The covariance matrix was also obtained from systematic variations due to the aforementioned corrections to the moments. The method assumes 100% correlation of any two truncated moments due to any single systematic variation. The covariance matrices that are derived from statistics and systematics are added to yield the overall covariance matrix, from which the correlations between any of the truncated moments are deduced. Tables V, VI, and VII show the correlation coefficients derived from this study.

To cross-check these moment measurements, we extract the moments from the Kagan-Neubert (KN) photon spectrum [14] tuned to fit our data [18] (m_b(KN) = 4.62 GeV,

TABLE V. Correlation coefficients between the $\langle E_\gamma \rangle$ measurements.

	$E_{\rm min}$ (GeV)	$\langle E_\gamma \rangle$ 1.8	1.9	2.0	2.1	2.2	2.3
	1.8	1.00	0.79	0.68	0.56	0.38	0.22
	1.9		1.00	0.82	0.70	0.52	0.33
$\langle E_\gamma \rangle$	2.0			1.00	0.86	0.67	0.47
	2.1				1.00	0.84	0.65
	2.2					1.00	0.86
	2.3						1.00

TABLE VI. Correlation coefficients between the $\langle E_\gamma \rangle$ and $\langle (E_\gamma - \langle E_\gamma \rangle)^2 \rangle$ measurements.

	$E_{\rm min}$ (GeV)	$\langle (E_\gamma - \langle E_\gamma \rangle)^2 \rangle$ 1.8	1.9	2.0	2.1	2.2	2.3
	1.8	−0.46	−0.18	−0.01	0.04	0.01	−0.01
	1.9	−0.06	−0.21	0.05	0.12	0.10	0.07
$\langle E_\gamma \rangle$	2.0	−0.14	0.15	0.12	0.23	0.20	0.17
	2.1	0.27	0.37	0.43	0.42	0.39	0.34
	2.2	0.38	0.55	0.67	0.75	0.66	0.61
	2.3	0.43	0.63	0.79	0.91	0.88	0.79

TABLE VII. Correlation coefficients between the $\langle (E_\gamma - \langle E_\gamma \rangle)^2 \rangle$ measurements.

$E_{\rm min}$ (GeV)		$\langle (E_\gamma - \langle E_\gamma \rangle)^2 \rangle$					
		1.8	1.9	2.0	2.1	2.2	2.3
$\langle (E_\gamma - \langle E_\gamma \rangle)^2 \rangle$	1.8	1.00	0.72	0.63	0.49	0.39	0.30
	1.9		1.00	0.83	0.71	0.61	0.52
	2.0			1.00	0.89	0.80	0.71
	2.1				1.00	0.96	0.91
	2.2					1.00	0.97
	2.3						1.00

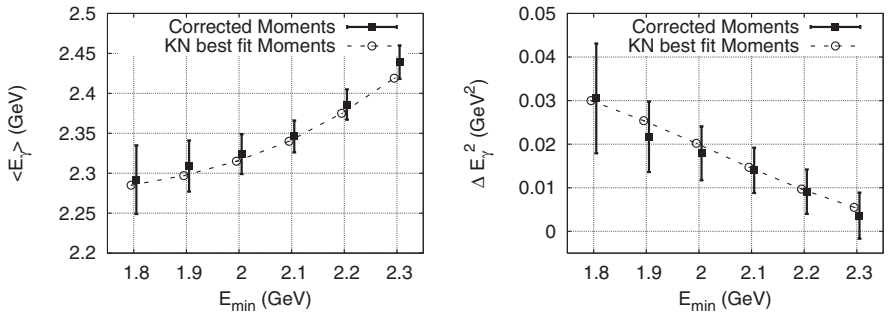

FIG. 3. Cross-check of the moment measurements. The moment measurements presented here are compared to the moments predicted in the Kagan-Neubert prescription, tuned to fit our data ($\Delta E_\gamma^2 = \langle (E_\gamma - \langle E_\gamma \rangle)^2 \rangle$).

$\mu_\pi^2({\rm KN}) = 0.40\ {\rm GeV}^2$). We generate the photon spectrum in the rest frame of the B meson with these parameters and extract the moments in the range $E_{\rm min} = 1.8, \ldots, 2.3$ GeV. The results are plotted in Fig. 3 along with the moment measurements presented here. We find very good agreement between these independent methods.

III. EXTRACTION OF $|V_{cb}|$ AND m_b FROM INCLUSIVE B DECAYS

A. Experimental inputs

Belle has measured the partial branching fractions $\Delta\mathcal{B}$ and the first, second, third, and fourth moments of the truncated electron energy spectrum in $B \to X_c e \nu$, $\langle E_\ell \rangle$, $\langle (E_\ell - \langle E_\ell \rangle)^2 \rangle$, $\langle (E_\ell - \langle E_\ell \rangle)^3 \rangle$, and $\langle (E_\ell - \langle E_\ell \rangle)^4 \rangle$ for nine different electron energy thresholds ($E_{\rm min} = 0.4$, 0.6, 0.8, 1.0, 1.2, 1.4, 1.6, 1.8, and 2.0 GeV) [10]. This analysis uses $\Upsilon(4S) \to B\bar{B}$ events equivalent to 140 fb^{-1} of integrated luminosity. The hadronic decay of one B meson is fully reconstructed and $B \to X_c e \nu$ decays of the other B are selected by requiring an identified electron amongst the particles remaining in the event.

In addition, Belle has measured the first, second central, and second noncentral moments of the hadron invariant mass squared (M_X^2) spectrum in $B \to X_c \ell \nu$, $\langle M_X^2 \rangle$, $\langle (M_X^2 - \langle M_X^2 \rangle)^2 \rangle$, and $\langle M_X^4 \rangle$ for seven different lepton energy thresholds ($E_{\rm min} = 0.7$, 0.9, 1.1, 1.3, 1.5, 1.7, and 1.9 GeV) [11]. This analysis is also based on 140 fb^{-1} of $\Upsilon(4S)$ data. Again, one B meson is fully reconstructed and a charged lepton (electron or muon) from the decay of the other B is required. The hadronic X_c system is reconstructed by summing the 4-momenta of the particles remaining in the event.

The measurements of the first and second moments of the photon energy spectrum in $B \to X_s \gamma$, $\langle E_\gamma \rangle$, and $\langle (E_\gamma - \langle E_\gamma \rangle)^2 \rangle$ have been described previously in this document. They are available for six different photon energy thresholds ($E_{\rm min} = 1.8$, 1.9, 2.0, 2.1, 2.2, and 2.3 GeV).

Hence, there are a total of 71 Belle measurements of inclusive spectra in B decays available for the global analysis [19]. The measurements actually used in the 1S and kinetic mass scheme fit analyses are shown in Table VIII: We have excluded measurements that do not have corresponding theoretical predictions; measurements with high $E_{\rm min}$ cutoffs (i.e., electron energy and hadronic mass moments with $E_{\rm min} > 1.5$ GeV and photon energy moments with $E_{\rm min} > 2$ GeV) are not used to determine the HQ parameters, as theoretical expressions are not considered reliable in this region [8,20]; finally, we have also excluded measurements where correlations with neighboring points are too high as these measurements do not add new information to the fit and introduce numerical problems such as negative eigenvalues of the covariance matrix.

TABLE VIII. Experimental inputs used in the 1S and kinetic mass scheme analyses. Both analyses use a total of 25 measurements.

	Measurements used
Lepton energy moments $\langle E_\ell^n \rangle$	$n = 0$: $E_{\rm min} = 0.6, 1.0, 1.4$ GeV $n = 1$: $E_{\rm min} = 0.6, 0.8, 1.0, 1.2, 1.4$ GeV $n = 2$: $E_{\rm min} = 0.6, 1.0, 1.4$ GeV $n = 3$: $E_{\rm min} = 0.8, 1.0, 1.2$ GeV
Hadronic mass moments $\langle M_X^{2n} \rangle$	$n = 1$: $E_{\rm min} = 0.7, 1.1, 1.3, 1.5$ GeV $n = 2$: $E_{\rm min} = 0.7, 0.9, 1.3$ GeV
Photon energy moments $\langle E_\gamma^n \rangle$	$n = 1$: $E_{\rm min} = 1.8, 2.0$ GeV $n = 2$: $E_{\rm min} = 1.8, 2.0$ GeV

The value of $|V_{cb}|$ is dependent on the average lifetime τ_B of neutral and charged B mesons. In the following analyses we use $\tau_B = (1.585 \pm 0.006)$ ps based on Ref. [21] and assume equal production of charged and neutral B mesons.

B. 1S mass scheme analysis

1. Theoretical input

The parameters appearing in the OPE depend on the choice of the mass scheme, i.e., the definition of m_b. The 1S scheme eliminates the b-quark pole mass by relating it to the mass of the $\Upsilon(1S)$. Truncated spectral moments in $B \to X_c \ell \nu$ have been derived in this scheme up to $\mathcal{O}(1/m_b^3)$ [2]. The theoretical expressions are of the form

$$\begin{aligned}\langle X \rangle_{E_{\rm min}} = {} & X^{(1)} + X^{(2)}\Lambda + X^{(3)}\Lambda^2 + X^{(4)}\Lambda^3 + X^{(5)}\lambda_1 \\ & + X^{(6)}\Lambda\lambda_1 + X^{(7)}\lambda_2 + X^{(8)}\Lambda\lambda_2 + X^{(9)}\rho_1 \\ & + X^{(10)}\rho_2 + X^{(11)}\tau_1 + X^{(12)}\tau_2 + X^{(13)}\tau_3 \\ & + X^{(14)}\tau_4 + X^{(15)}\epsilon + X^{(16)}\epsilon_{\rm BLM}^2 + X^{(17)}\epsilon\Lambda,\end{aligned} \tag{1}$$

where $\langle X \rangle$ stands for any experimental observable in Table VIII and $X^{(i)}$, $i = 1, \ldots, 17$, are perturbatively calculable coefficients that depend on $E_{\rm min}$. The computations include radiative contributions of $\mathcal{O}(\epsilon)$ and $\mathcal{O}(\epsilon_{\rm BLM}^2)$, the so-called Brodsky-Lepage-Mackenzie (BLM) contribution at $\mathcal{O}(\epsilon^2)$. The HQ parameters are Λ at leading order, λ_1 and λ_2 at $\mathcal{O}(1/m_b^2)$, and τ_1, τ_2, τ_3, τ_4, ρ_1, and ρ_2 at $\mathcal{O}(1/m_b^3)$. The CKM magnitude $|V_{cb}|$ enters through the predictions of the partial semileptonic branching fractions,

$$\Delta\mathcal{B}_{E_{\rm min}} = \frac{G_F^2 m^5}{192\pi^3}|V_{cb}|^2 \eta_{\rm QED}\tau_B \langle X \rangle_{\Delta\mathcal{B}, E_{\rm min}}, \tag{2}$$

where m is the 1S reference mass, $m = m_{\Upsilon(1S)}/2$, $G_F^2 m^5/(192\pi^3) = 5.4 \times 10^{-11}$ ps^{-1}, $\eta_{\rm QED} = 1.007$, and $\langle X \rangle_{\Delta\mathcal{B}, E_{\rm min}}$ is an expression of the form of Eq. (2).

The analysis in the 1S mass scheme determines a total of seven parameters: $|V_{cb}|$, Λ, λ_1, τ_1, τ_2, τ_3, and ρ_1. Following the prescriptions in Ref. [2], τ_4 is set to zero and the measured $B^* - B$ and $D^* - D$ mass splittings allow us to constrain some of the HQET matrix elements in Eq. (2): $\lambda_2 = 0.1227 - 0.0145\lambda_1$ and $\rho_2 = 0.1361 + \tau_2$. The parameter Λ is the difference between the b-quark and the reference mass, $\Lambda = m_{\Upsilon(1S)}/2 - m_b^{\rm 1S}$. We will present our results in terms of $m_b^{\rm 1S}$.

2. The fit

The expressions in the 1S scheme are fitted to the data using the χ^2 minimization technique and the MINUIT program [22]. The covariance matrix used in the fit takes into account both experimental and theoretical uncertainties. Following the approach in Ref. [2], an element of the combined experimental and theoretical error matrix is given by

$$\sigma_{ij}^2 = \sigma_i \sigma_j c_{ij}, \tag{3}$$

where i and j denote the observables and c_{ij} is the experimental correlation matrix element. The total error on the observable i is defined as

$$\begin{aligned}\sigma_i &= \sqrt{(\sigma_i^{\rm exp})^2 + (A f_n m_B^{2n})^2 + (B_i/2)^2} \\ &\quad \text{for the } n\text{th hadron moment,} \\ \sigma_i &= \sqrt{(\sigma_i^{\rm exp})^2 + (A f_n (m_B/2)^n)^2 + (B_i/2)^2} \\ &\quad \text{for the } n\text{th lepton moment,} \\ \sigma_i &= \sqrt{(\sigma_i^{\rm exp})^2 + (A f_n (m_B/2)^n)^2 + (B_i/2)^2} \\ &\quad \text{for the } n\text{th photon moment,}\end{aligned} \tag{4}$$

and $f_0 = f_1 = 1$, $f_2 = 1/4$, and $f_3 = 1/(6\sqrt{3})$. Here, $\sigma_i^{\rm exp}$ are the experimental errors, $B_i = X^{(16)}$ are the coefficients of the last computed terms in the perturbation series (used to estimate the uncertainty on the uncalculated higher order perturbative terms), and A is a dimensionless parameter that contains different theoretical uncertainties [uncalculated power corrections, uncalculated effects of order $(\alpha_s/4\pi)\Lambda_{\rm QCD}^2/m_b^2$, and effects not included in the OPE, i.e., duality violation]. For lepton and hadron moments, we

TABLE IX. Result of fit in the 1S mass scheme. The σ(fit) error contains the experimental and theoretical uncertainties in the moments. The $\sigma(\tau_B)$ error on $|V_{cb}|$ is due to the uncertainty in the average B meson lifetime. In the lower part of the table, the correlation matrix of the parameters is given.

	$\lvert V_{cb}\rvert$ (10^{-3})	m_b (GeV)	λ_1 (GeV^2)	ρ_1 (GeV^3)	τ_1 (GeV^3)	τ_2 (GeV^3)	τ_3 (GeV^3)
Value	41.56	4.723	−0.303	0.067	0.125	−0.101	0.125
σ(fit)	0.68	0.055	0.046	0.030	0.005	0.056	0.005
$\sigma(\tau_B)$	0.08						
$\lvert V_{cb}\rvert$	1.000	−0.121	0.003	0.195	0.008	−0.432	0.021
m_b		1.000	0.893	−0.137	−0.002	−0.509	−0.006
λ_1			1.000	−0.410	−0.041	−0.429	−0.045
ρ_1				1.000	0.009	−0.533	0.028
τ_1					1.000	0.005	0.000
τ_2						1.000	0.007
τ_3							1.000

fix $A = 0.001$ [2]. For photon moments, the factor A is 0.001 multiplied by the ratio of the energy difference from the endpoint, relative to that for $E_{\rm min} = 1.8$ GeV, to account for the increase in shape function effects as one limits the allowed region of the photon spectrum.

As the fit does not provide strong constraints on the $1/m_b^3$ parameters, we add the following extra terms to the χ^2 function:

$$\chi^2_{\langle\mathcal{O}\rangle} = \begin{cases} 0 & |\langle\mathcal{O}\rangle| \le m_\chi^3, \\ (|\langle\mathcal{O}\rangle| - m_\chi^3)^2/M_\chi^6 & |\langle\mathcal{O}\rangle| > m_\chi^3, \end{cases} \quad (5)$$

where (m_χ, M_χ) are both quantities of $\mathcal{O}(\Lambda_{\rm QCD})$, and $\langle\mathcal{O}\rangle$ are the matrix elements of any of the $\mathcal{O}(1/m_b^3)$ operators in the fit. For the central value of the fit, we take $M_\chi = m_\chi = 500$ MeV [2].

3. Results and discussion

The results for the fit parameters are given in Table IX. Using the measurement of the partial branching fraction at $E_{\rm min} = 0.6$ GeV, we obtain for the semileptonic branching fraction (over the full lepton energy range) $\mathcal{B}_{X_c\ell\nu} = (10.60 \pm 0.28)\%$. A comparison of the measured moments and the 1S scheme predictions is shown in Figs. 4 and 5.

We have verified the stability of the fit by considering the following variations (Table X): (a) by repeating the fit

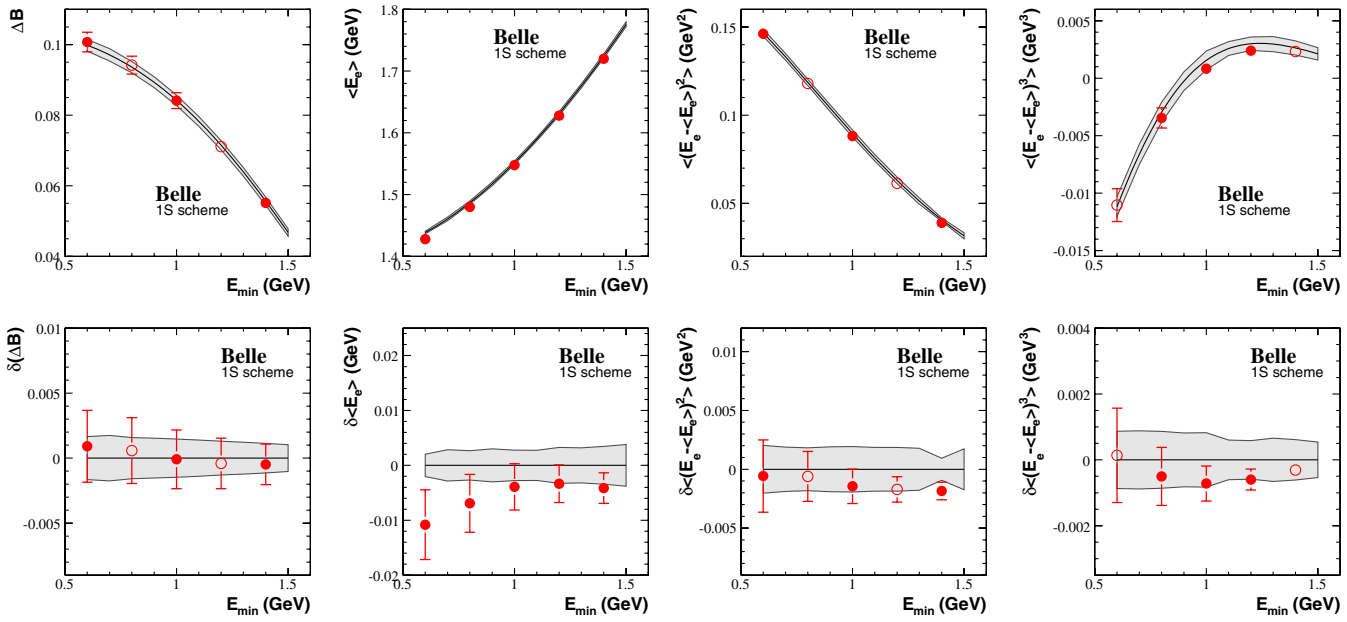

FIG. 4 (color online). Comparison of the measured electron energy moments and the 1S scheme predictions (upper row), and difference between the measurements and the predictions (lower row). The error bars show the experimental uncertainties. The error bands represent the theory error. Filled circles are data points used in the fit, and open circles are unused measurements.

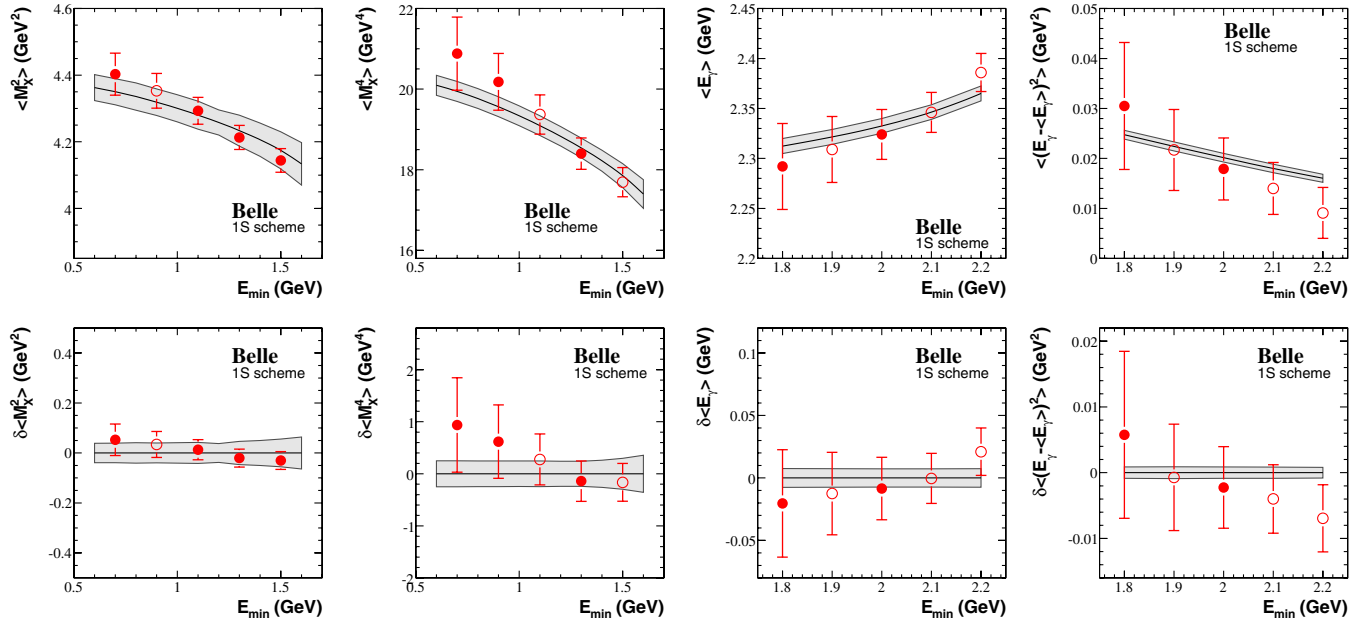

FIG. 5 (color online). Same as Fig. 4 for the measured hadronic mass and photon energy moments and the 1S scheme predictions.

TABLE X. Stability of the fit in the 1S mass scheme. The different setups are explained in the text. Setup (d) corresponds to the default fit.

Setup	χ^2/ndf.	$\lvert V_{cb}\rvert$ (10^{-3})	m_b (GeV)	λ_1 (GeV^2)
(a)	6.4/14	41.55 ± 0.80	4.718 ± 0.119	-0.308 ± 0.092
(b)	5.6/18	41.28 ± 0.86	4.699 ± 0.060	-0.491 ± 0.084
(c)	16.6/18	41.10 ± 0.54	4.666 ± 0.046	-0.341 ± 0.031
(d)	7.3/18	41.56 ± 0.68	4.723 ± 0.055	-0.303 ± 0.046

only for the $B \to X_c \ell \nu$ data (21 measurements); (b) by releasing the m_χ constraint on the higher order parameters; (c) by repeating the fit with all theoretical uncertainties set to zero. In Table X the default fit corresponds to setup (d). Figure 6 shows the $\Delta\chi^2 = 1$ contour plots for the fits corresponding to setups (a) and (d) in Table X.

C. Kinetic mass scheme analysis

1. Theoretical input

Spectral moments of the lepton energy and hadronic mass in $B \to X_c \ell \nu$ decays have been derived in the kinetic mass scheme up to $\mathcal{O}(1/m_b^3)$ [7]. Compared to the original publication, the theoretical expressions in our fit contain an

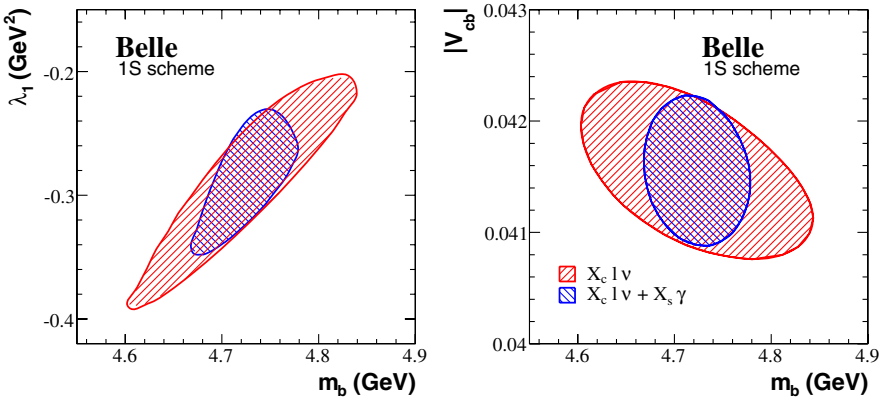

FIG. 6 (color online). $\Delta\chi^2 = 1$ contours for the fit to all moments and the fit to the $B \to X_c \ell \nu$ data only.

improved calculation of the perturbative corrections to the lepton energy moments [23] and account for the $E_{\rm min}$ dependence of the perturbative corrections to the hadronic mass moments [24]. For the photon energy moments in $B \to X_s\gamma$, the (biased) OPE prediction and the bias correction have been calculated [8].

These expressions depend on the following set of nonperturbative parameters: the b- and c-quark masses m_b and m_c, μ_π^2 and μ_G^2 at $\mathcal{O}(1/m_b^2)$ and $\tilde{\rho}_D^3$ and ρ_{LS}^3 at $\mathcal{O}(1/m_b^3)$ [25]. In our analysis, we determine these six parameters together with the semileptonic branching fraction (over the full lepton energy range) $\mathcal{B}_{X_c\ell\nu}$. The total number of parameters in the fit is thus seven.

The CKM magnitude $|V_{cb}|$ is calculated using the following expression [6]:

$$\begin{aligned}\frac{|V_{cb}|}{0.0417} = &\left(\Gamma(B \to X\ell\nu)\frac{1.55\ \text{ps}}{0.105}\right)^{1/2}[1 + 0.30(\alpha_s - 0.22)] \\ &\times [1 - 0.66(m_b - 4.6\ \text{GeV}) \\ &+ 0.39(m_c - 1.15\ \text{GeV}) \\ &+ 0.013(\mu_\pi^2 - 0.4\ \text{GeV}^2) \\ &+ 0.09(\tilde{\rho}_D^3 - 0.1\ \text{GeV}^3) \\ &+ 0.05(\mu_G^2 - 0.35\ \text{GeV}^2) \\ &- 0.01(\rho_{LS}^3 + 0.15\ \text{GeV}^3)], \end{aligned} \tag{6}$$

where $\Gamma(B \to X\ell\nu)$ is the semileptonic width of the B meson.

2. The fit

As in the 1S scheme case, the fit is performed using the χ^2 minimization technique and the MINUIT program [22]. The covariance matrix used is the sum of matrices corresponding to the experimental and theoretical uncertainties. The theoretical covariance matrix is constructed following the recipe in Ref. [7]:

The nonperturbative uncertainties (i.e., the uncertainties related to the $1/m_b$ expansion) are evaluated by varying μ_π^2 and μ_G^2 ($\tilde{\rho}_D^3$ and ρ_{LS}^3) by $\pm 20\%$ ($\pm\ 30\%$) around their "nominal" values of $\mu_\pi^2 = 0.4\ \text{GeV}^2$, $\tilde{\rho}_D^3 = 0.1\ \text{GeV}^3$, $\mu_G^2 = 0.35\ \text{GeV}^2$, and $\rho_{LS}^3 = -0.15\ \text{GeV}^3$. The perturbative uncertainties (i.e., the uncertainties related to the expansion in α_s) are estimated by varying α_s within ± 0.04 ($\pm\ 0.1$) around the central value of 0.22 (0.3) for the lepton and photon energy (hadronic mass) moments. The difference in the treatment of α_s for the hadronic mass moments is due to the fact that the calculation of the perturbative corrections to these moments is less complete.

The theoretical uncertainty in the moment predictions is the quadratic sum of these different contributions. The theoretical covariance matrix is then constructed by treating these errors as fully correlated for a given moment with different $E_{\rm min}$ while they are treated as uncorrelated between moments of different order.

For the moments of the photon energy spectrum, we take 30% of the absolute value of the bias correction as its uncertainty. This additional theoretical error is considered uncorrelated for moments with different $E_{\rm min}$ and different order.

The experimental data from $B^* - B$ mass splitting and heavy quark sum rules constrain the parameters μ_G^2 and ρ_{LS}^3 to $0.35 \pm 0.07\ \text{GeV}^2$ and $-0.15 \pm 0.1\ \text{GeV}^3$, respectively. We account for these constraints by adding the following additional terms to the χ^2 function:

$$\begin{aligned}&(\mu_G^2 - 0.35\ \text{GeV}^2)^2/(0.07\ \text{GeV}^2)^2 \\ &\quad + (\rho_{LS}^3 + 0.15\ \text{GeV}^3)^2/(0.1\ \text{GeV}^3)^2. \end{aligned} \tag{7}$$

To calculate $|V_{cb}|$ using Eq. (6) and properly account for the correlations of the HQ parameters, we make $|V_{cb}|$ a free parameter of the fit, calculate $\Gamma(B \to X_c\ell\nu)$ with Eq. (6)

TABLE XI. Result of fit in the kinetic mass scheme. The σ(fit) error contains the experimental and theoretical uncertainties in the moments. The $\sigma(\tau_B)$ and σ(th) errors on $|V_{cb}|$ are due to the uncertainty in the average B meson lifetime and the limited accuracy of Eq. (6), respectively. In the lower part of the table, the correlation matrix of the parameters is given.

	$\lvert V_{cb}\rvert$ (10^{-3})	m_b (GeV)	m_c (GeV)	μ_π^2 (GeV^2)	$\tilde{\rho}_D^3$ (GeV^3)	μ_G^2 (GeV^2)	ρ_{LS}^3 (GeV^3)
Value	41.58	4.543	1.055	0.539	0.166	0.362	−0.153
σ(fit)	0.69	0.075	0.118	0.079	0.040	0.053	0.096
$\sigma(\tau_B)$	0.08						
σ(th)	0.58						
$\lvert V_{cb}\rvert$	1.000	−0.371	−0.316	0.511	0.493	−0.166	0.073
m_b		1.000	0.988	−0.783	−0.702	−0.178	−0.187
m_c			1.000	−0.771	−0.715	−0.262	−0.108
μ_π^2				1.000	0.777	0.205	0.080
$\tilde{\rho}_D^3$					1.000	0.108	−0.158
μ_G^2						1.000	−0.103
ρ_{LS}^3							1.000

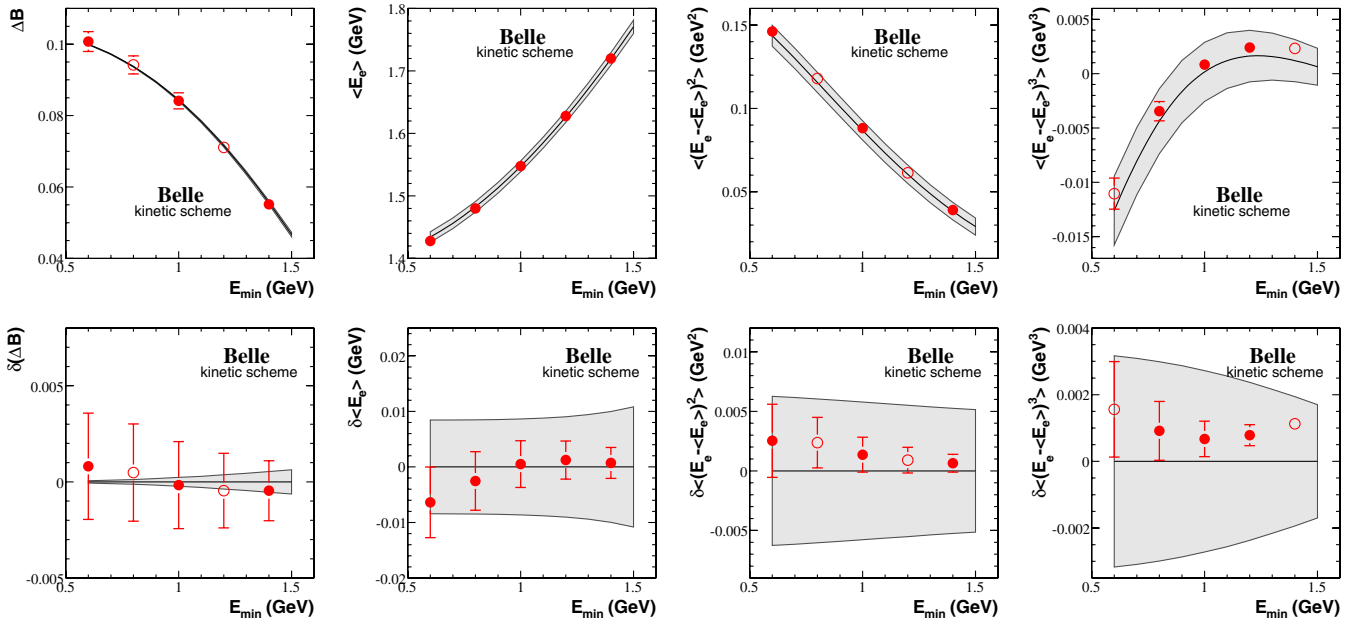

FIG. 7 (color online). Comparison of the measured electron energy moments and the kinetic scheme predictions (upper row), and difference between the measurements and the predictions (lower row). The error bars show the experimental uncertainties. The error bands represent the theory error. Filled circles are data points used in the fit, and open circles are unused measurements.

and add the following term to the χ^2 function:

$$\left(\frac{\mathcal{B}_{X_c\ell\nu}}{\Gamma(B\to X_c\ell\nu)}-\tau_B\right)^2/\sigma^2. \qquad (8)$$

The uncertainty σ accounts for the experimental uncertainty in τ_B and an additional 1.4% theoretical uncertainty in extracting $|V_{cb}|$ using Eq. (6) [6]. We have verified that this method of calculating $|V_{cb}|$ does not change the fit result for the other parameters.

3. Results and discussion

The results of the fit in the kinetic mass scheme are shown in Table XI. The value of the χ^2 function at the minimum is 4.7 for $25-7$ degrees of freedom. The semi-

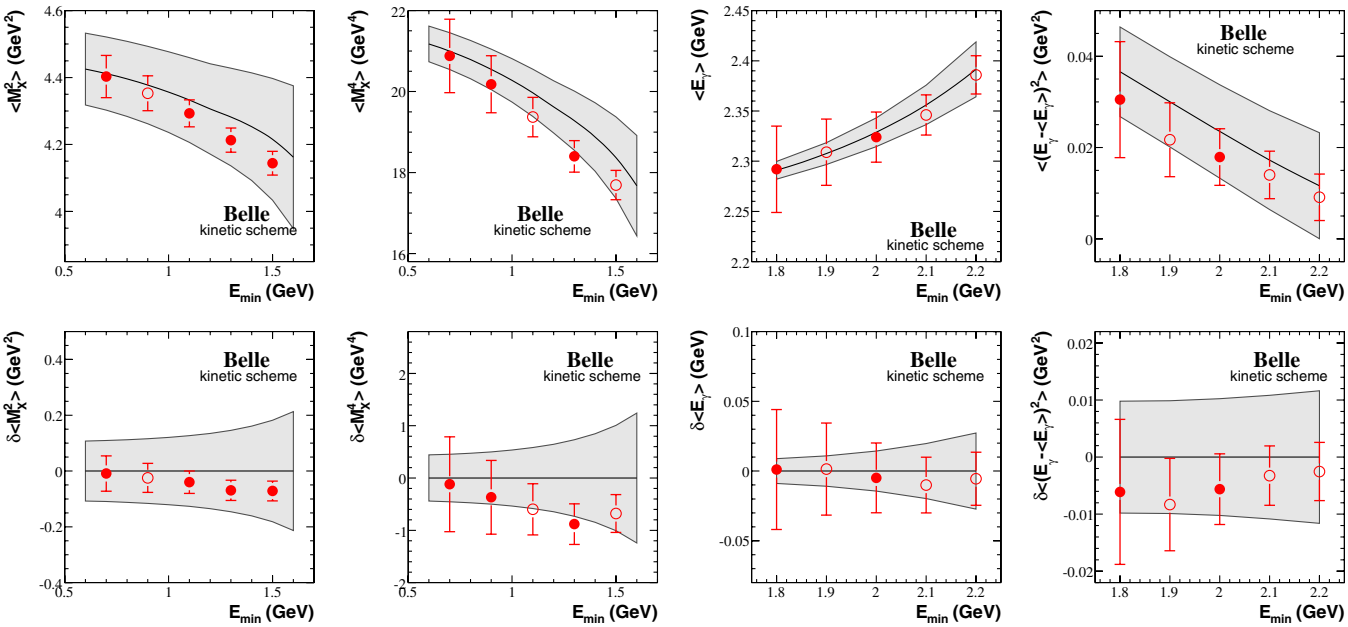

FIG. 8 (color online). Same as Fig. 7 for the measured hadronic mass and photon energy moments and the kinetic scheme predictions.

TABLE XII. Stability of the fit in the kinetic mass scheme. Setup (a) uses the $B \to X_c \ell \nu$ data only; setup (b) corresponds to the default fit.

Setup	χ^2/ndf.	$\lvert V_{cb}\rvert$ (10^{-3})	m_b (GeV)	μ_π^2 (GeV^2)
(a)	4.2/14	41.51 ± 0.99	4.573 ± 0.134	0.523 ± 0.106
(b)	4.7/18	41.58 ± 0.90	4.543 ± 0.075	0.539 ± 0.079

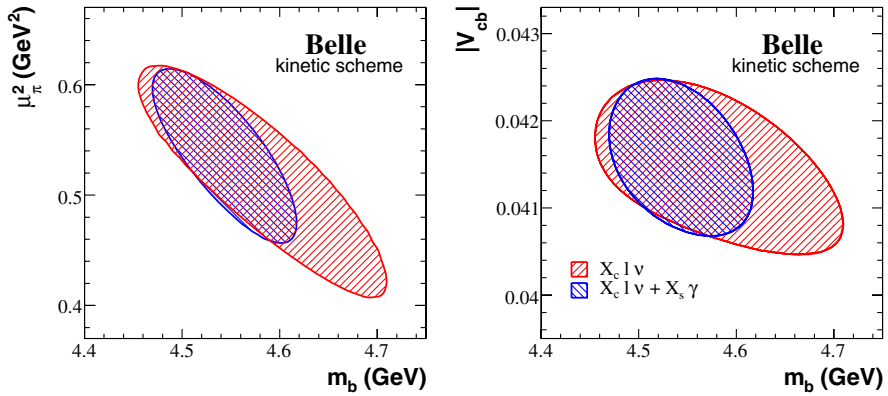

FIG. 9 (color online). $\Delta\chi^2 = 1$ contours for the fit to all moments and the fit to the $B \to X_c \ell \nu$ data only.

leptonic branching fraction $\mathcal{B}_{X_c \ell \nu}$ is found to be (10.49 ± 0.23)%. The comparison of the measurements and the predictions in the kinetic scheme is shown in Figs. 7 and 8.

We have repeated the fit using the $B \to X_c \ell \nu$ moments only, excluding $B \to X_s \gamma$ data (Table XII). Figure 9 shows the $\Delta\chi^2 = 1$ contour plots for the fits corresponding to setups (a) and (b) in Table XII.

IV. SUMMARY

We have determined the first and second moments of the photon energy distribution in $B \to X_s \gamma$ decays, $\langle E_\gamma \rangle$ and $\langle (E_\gamma - \langle E_\gamma \rangle)^2 \rangle$, for minimum photon energies in the B meson rest frame ranging from 1.8 to 2.3 GeV using the measurement of this spectrum published in Ref. [9]. The results are given in Table IV. We have also evaluated the (statistical and systematic) self-correlations and cross correlations between these measurements (Tables V, VI, and VII).

In the second part of the present document, we have combined these measurements with recent Belle data on the lepton energy and hadronic mass moments in $B \to X_c \ell \nu$ decays [10,11] to extract $|V_{cb}|$, m_b and other nonperturbative parameters using theoretical expressions derived in the 1S [2] and kinetic [7,8] schemes.

The fits give consistent values of $|V_{cb}|$ in the two schemes. In the 1S scheme analysis we find $|V_{cb}| = (41.56 \pm 0.68(\text{fit}) \pm 0.08(\tau_B)) \times 10^{-3}$ and $m_b^{1S} = (4.723 \pm 0.055)$ GeV. In the kinetic scheme, we obtain $|V_{cb}| = (41.58 \pm 0.69(\text{fit}) \pm 0.08(\tau_B) \pm 0.58(\text{th})) \times 10^{-3}$ and $m_b^{\text{kin}} = (4.543 \pm 0.075)$ GeV. Note that the m_b values can only be compared after scheme translation. The fit results using only the $B \to X_c \ell \nu$ data are $|V_{cb}| = (41.55 \pm 0.80(\text{fit}) \pm 0.08(\tau_B)) \times 10^{-3}$ and $m_b^{1S} = (4.718 \pm 0.119)$ GeV in the 1S scheme, and $|V_{cb}| = (41.51 \pm 0.80(\text{fit}) \pm 0.08(\tau_B) \pm 0.58(\text{th})) \times 10^{-3}$ and $m_b^{\text{kin}} = (4.573 \pm 0.134)$ GeV in the kinetic scheme (see Tables X and XII).

The CKM magnitude $|V_{cb}|$ and the b-quark masses $m_b^{\text{kin,1S}}$ have been extracted with values that are consistent with previous determinations [2–5]. In the 1S scheme $|V_{cb}|$ has been measured with 1.6% precision. This is the most precise determination by any single experiment so far [4,5].

ACKNOWLEDGMENTS

We thank the theorists working on the 1S scheme: C. W. Bauer, Z. Ligeti, M. Luke, A. V. Manohar, and M. Trott, and those working on the kinetic scheme: P. Gambino, N. Uraltsev, and I. Bigi for providing the Mathematica and Fortran codes that describe the respective calculations. We thank the KEKB group for the excellent operation of the accelerator, the KEK cryogenics group for the efficient operation of the solenoid, and the KEK computer group and the National Institute of Informatics for valuable computing and SINET3 network support. We acknowledge support from the Ministry of Education, Culture, Sports, Science, and Technology of Japan and the Japan Society for the Promotion of Science; the Australian Research Council, the Australian Department of Education, Science and Training; the National Natural Science Foundation of China under Contracts No. 10575109 and No. 10775142; the Department of Science and Technology

of India; the BK21 program of the Ministry of Education of Korea, the CHEP SRC program and Basic Research program (Grant No. R01-2005-000-10089-0) of the Korea Science and Engineering Foundation, and the Pure Basic Research Group program of the Korea Research Foundation; the Polish State Committee for Scientific Research; the Ministry of Education and Science of the Russian Federation and the Russian Federal Agency for Atomic Energy; the Slovenian Research Agency; the Swiss National Science Foundation; the National Science Council and the Ministry of Education of Taiwan; and the U.S. Department of Energy.

[1] N. Cabibbo, Phys. Rev. Lett. **10**, 531 (1963); M. Kobayashi and T. Maskawa, Prog. Theor. Phys. **49**, 652 (1973).
[2] C. W. Bauer, Z. Ligeti, M. Luke, A. V. Manohar, and M. Trott, Phys. Rev. D **70**, 094017 (2004).
[3] O. Buchmuller and H. Flacher, Phys. Rev. D **73**, 073008 (2006).
[4] J. Abdallah *et al.* (DELPHI Collaboration), Eur. Phys. J. C **45**, 35 (2006).
[5] B. Aubert *et al.* (*BABAR* Collaboration), arXiv:0707.2670.
[6] D. Benson, I. I. Bigi, T. Mannel, and N. Uraltsev, Nucl. Phys. **B665**, 367 (2003).
[7] P. Gambino and N. Uraltsev, Eur. Phys. J. C **34**, 181 (2004).
[8] D. Benson, I. I. Bigi, and N. Uraltsev, Nucl. Phys. **B710**, 371 (2005).
[9] P. Koppenburg *et al.* (Belle Collaboration), Phys. Rev. Lett. **93**, 061803 (2004).
[10] P. Urquijo *et al.*, Phys. Rev. D **75**, 032001 (2007).
[11] C. Schwanda *et al.* (Belle Collaboration), Phys. Rev. D **75**, 032005 (2007).
[12] R. A. Fisher, Annals Eugen. **7**, 179 (1936).
[13] G. C. Fox and S. Wolfram, Phys. Rev. Lett. **41**, 1581 (1978).
[14] A. L. Kagan and M. Neubert, Eur. Phys. J. C **7**, 5 (1999).
[15] S. Nishida *et al.* (BELLE Collaboration), Phys. Rev. Lett. **93**, 031803 (2004).
[16] S. Chen *et al.* (CLEO Collaboration), Phys. Rev. Lett. **87**, 251807 (2001).
[17] B. Aubert *et al.* (*BABAR* Collaboration), Phys. Rev. D **72**, 052004 (2005).
[18] A. Limosani and T. Nozaki (Heavy Flavor Averaging Group), arXiv:hep-ex/0407052.
[19] The measurements of $\langle M_X^4 \rangle$ and $\langle (M_X^2 - \langle M_X^2 \rangle)^2 \rangle$ correspond to the same order in M_X^2 and are counted only once.
[20] N. Uraltsev, in Proceedings of the 2nd Workshop on the CKM Unitarity Triangle, Durham, England, 2003, p. WG118.
[21] E. Barberio *et al.* (Heavy Flavor Averaging Group (HFAG) Collaboration), arXiv:0704.3575.
[22] F. James and M. Roos, Comput. Phys. Commun. **10**, 343 (1975).
[23] P. Gambino (private communication).
[24] N. Uraltsev, Int. J. Mod. Phys. A **20**, 2099 (2005).
[25] In this analysis, all nonperturbative parameters in the kinetic scheme are defined at the scale $\mu = 1$ GeV.